http://dx.doi.org/10.5012/bkcs.2014.35.1.57

Effect of Activation Temperature on CO_2 Capture Behaviors of Resorcinol-based Carbon Aerogels

Cheol-Whan Moon, Youngjoo Kim,† Seung-Soon Im, and Soo-Jin Park†,*

Department of Organic and Nano Engineering, Hanyang University, Seoul, Korea
*†Department of Chemistry, Inha University, Incheon, Korea. *E-mail: sjpark@inha.ac.kr*
Received August 28, 2013, Accepted October 4, 2013

In this study, carbon aerogel (CA) was synthesized using a soft-template method, and the optimum conditions for the adsorption of carbon dioxide (CO_2) by the carbon aerogel were evaluated by controlling the activation temperature. KOH was used as the activation agent at a KOH/CA activation ratio of 4:1. Three types of activated CAs were synthesized at activation temperatures of 800 °C (CA-K-800), 900 °C (CA-K-900), and 1000 °C (CA-K-1000), and their surface and pore characteristics along with the CO_2 adsorption characteristics were examined. The results showed that with the increase in activation temperature from 800 to 900 °C, the total pore volume and specific surface area sharply increased from 1.2165 to 1.2500 cm^3/g and 1281 to 1526 m^2/g, respectively. However, the values for both these parameters decreased at temperatures above 1000 °C. The best CO_2 adsorption capacity of 10.9 wt % was obtained for the CA-K-900 sample at 298 K and 1 bar. This result highlights the importance of the structural and textural characteristics of the carbon aerogel, prepared at different activation temperatures on CO_2 adsorption behaviors.

Key Words : Carbon dioxide adsorption, Activation temperature, Carbon aerogel, Soft-template method

Introduction

The volume of carbon dioxide (CO_2), a major cause of global warming, has been increasing because of a rapid increase in the use of fossil fuels driven by the recent industrial development. Extensive studies on CO_2 capture are underway to reduce such CO_2 emissions. Commonly used CO_2 capture methods include absorption, adsorption, and membrane separation; the absorption and adsorption methods are being intensively studied. The absorption method has been widely used to capture CO_2; however, it requires not only regular refills of absorption liquid but also requires regular equipment maintenance and repair because of corrosion and generation of secondary pollutants. Numerous studies have been conducted on dry solvents; however, a dry solvent has the drawback of being pulverized under the operating conditions of high temperature, high pressure, and flow friction of the dry solvent.[1] In contrast, adsorption is considered an economic method because minimum energy is consumed and because the adsorbent can be reused.[2,3] Numerous studies have focused on developing adsorbents that improve adsorption capacity because of the ease of application. The separation efficiency of CO_2 depends on the type of adsorbent, which includes carbon materials,[4-8] macroporous silica (SBA-15,[9] MCM-41[10]), and metallic oxides.[11-14] Carbon aerogels are the most popular CO_2 adsorbent[15] because of its large specific surface area; however, it has several drawbacks such as diminishing adsorption capacity at high temperature and low carbon selectivity.

Carbon aerogel (CA) is an important carbon material whose 3D-bonded network contains micropores with a size less than 2 nm, stable mesopores with sizes ranging from 2 nm to 50 nm, and a large specific surface area (400-1200 m^2/g).[16,17] Pekala prepared CAs by carbonization of a resorcinol-formaldehyde (RF) aerogel.[18,19] Such carbon materials can be prepared by hard- and soft-template methods. A hard template can be made up of a fragmented solid material of regular shape. Its advantage lies in the synthesis of carbon with a regular structure although the solid-phase materials need to be removed. Unlike hard templates, a soft template does not require the removal of solid-phase materials, which facilitates the synthesis of carbon.[20,21] Therefore, we chose to use a soft template for the synthesis of CAs owing to their facile fabrication process. The factors affecting CO_2 adsorption capacity, such as the shape, size, and pore distribution of the carbon material are controlled by different activation methods. The carbon materials can be activated by both physical and chemical methods although the chemical method is more popular due to many advantages. The chemical method uses acid and alkaline reagents such as KOH, Na_2CO_3, NaOH, $ZnCl_2$, $MgCl_2$, and H_3PO_4,[22-24] and among these reagents, KOH is the most widely used as it results in CAs of high specific surface area. In addition, temperature is an important factor in chemical activation; however, the optimum activation temperature required for improving CO_2 adsorption capacity has not yet been reported.

Therefore, we prepared activated CAs using KOH and evaluated the effect of activation temperature on CO_2 adsorption capacity by monitoring the specific surface area and changes in pore size and number after activating the CAs with KOH and measuring the resulting CO_2 adsorption capacity.

Experimental

Raw Materials and Experimental Methods. For the synthesis of CAs in this study, we used formaldehyde (Duksan Pure Chemicals, Korea) as the initiator, resorcinol as the carbon precursor, and Na_2CO_3 (Sigma-Aldrich, USA) as the catalyst. The carbon aerogels were activated (CA-K) by treating with KOH and heating at various carbonization temperatures.

For the synthesis of CAs, Na_2CO_3 and formaldehyde were added to a solution of resorcinol in distilled water. The resulting solution was solidified by stirring for 3 h and then heated in an oven at 80 °C for 48 h to induce gelation. The resulting wet gel was soaked in acetone at 50 °C to replace the water in the gel with acetone. The resulting gel was then dried in an oven for 24 h to completely remove the acetone. The dried aerogel was annealed for 5 h at 750 °C under a nitrogen atmosphere to yield CAs.

The CAs were activated as follows: CA and KOH in a weight ratio of 1:4 were added to 100 mL distilled water, stirred for 12 h at 80 °C, and then dried for 24 h at 80 °C. The dried substance was annealed in a tube furnace under nitrogen for 1 h by increasing the temperature at the speed of 2 °C/min from 800 °C to 1000 °C, at increments of 100 °C. In order to remove potassium ions and impurities after annealing, the substance was washed with 0.5 N HCl and further washed and filtered with distilled water until the filtrate became neutral. The final activated CAs, were named CA-K-800 through CA-K-1000 according to their respective processing temperatures.

Characteristics of the Surface and Pore Structure. Structural changes in the crystals of the CAs were measured by X-ray diffraction (XRD) (D2 Phaser, Bruker, Germany), and the surface characteristics and changes in the shape of the surface were examined using a scanning electron microscope (SEM, Hitachi S-4300SE, Japan). The specific surface area and pore structure were measured using a surface area and pore size analyzer (BELSORP Inc., Japan). The nitrogen sorption isotherms were obtained at 77 K. The BET (Brunauer-Emmett-Teller) equation was used to measure the specific surface area, and the total pore volume (V_t) was obtained from the nitrogen adsorption volume at $P/P_0 = 0.99$. The mesopore volume (V_m) was calculated by using the BJH (Barrett-Joyner-Halenda) equation, and the average pore diameter (D) from Eq. (1):

$$D(nm) = \frac{4V_t \times 1000}{S_{BET}} \quad (1)$$

CO_2 Adsorption Behaviors. The activated CAs thus produced were dehydrated and purified under vacuum by using volumetric technique, and while it remained in the vacuum, the temperature was lowered to the adsorption temperature. Then, we measured the change in the CO_2 adsorption volume with the relative pressure (P/P_0), at 298 K, which is a temperature at which the sample is stable.

Results and Discussion

Surface and Structure Characteristics of Activated CAs. XRD analysis was performed to characterize the microstructure and molecular structure of the crystal of KOH-treated CAs at different temperatures, and the result is shown in Figure 1. A unique hexagonal graphite peak at $2\theta = 23°$ and a rhombohedral graphite peak at $2\theta = 43°$ were observed.[25] Compared to the pre-activation CA sample, the KOH-treated CA (CA-K-800) showed a wide and asymmetric peak at $2\theta = 23°$, indicating an amorphous carbon.[26] Furthermore, for the KOH-treated CAs, the intensity of the (002) peak weakened with increasing treatment temperature, and the diffraction angle moved towards the base angle. The results from Figure 1 are summarized in Table 1. The 2θ values for the untreated CA, CA-K-800, and CA-K-900, were 24.02, 21.69, and 21.24°, respectively, whereas the 2θ value for CA-K-1000 was not measured. Table 1 lists the values of d_{002} (interlayer spacing) and 2θ (Bragg's angle), determined using Bragg's law, for the samples activated at various temperatures. The values are related to the structure of graphite and the size of the crystal, and the d_{002} values of the CA, CA-K-800, and CA-K-900 samples increased to 3.70, 4.09, and 4.17 Å, respectively, as the temperature increased. However, the d_{002} value was not measured for CA-K-1000. This result shows that the temperatures affected and changed the structures of the activated CAs.

Figure 2 shows the SEM images of the activated CAs. The number of irregular surface defects increased with temperature, and a structural change was observed for CA-K-1000. Thus, it appears that the chemical reactions between KOH and the CA at 1,000 °C affected the structure of the CA,

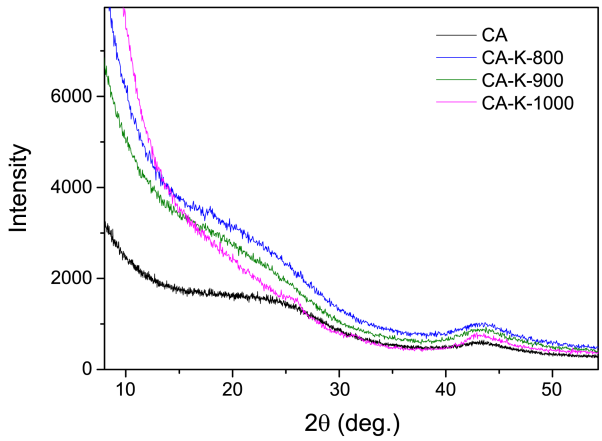

Figure 1. XRD patterns of the CAs synthesized at 800-1000 °C.

Table 1. Microstructural property of the activated carbons studied by XRD

Nomenclature	CA	CA-K-800	CA-K-900	CA-K-1000
$2\theta^a$	24.02	21.69	21.24	-
$d_{002}{}^b$	3.70	4.09	4.17	-

[a]Bragg angle. [b]Interlayer spacing

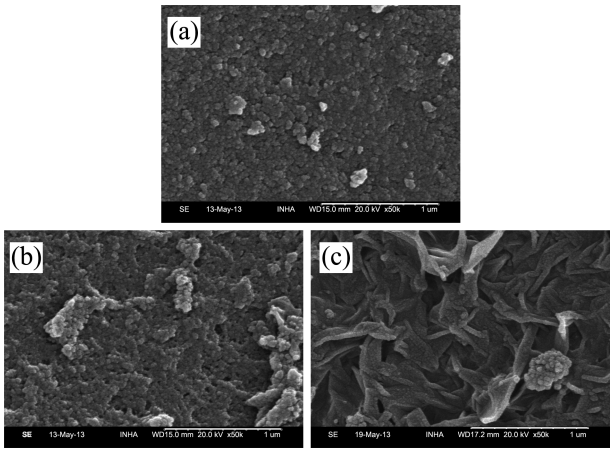

Figure 2. SEM images of the different CAs: (a) CA-K-800, (b) CA-K-900, and (c) CA-K-1000.

leading to pore shrinkage.[27] KOH permeated into the CAs and reacted with the carbon in CAs according to Eqs. (1)-(3) described below.

$$6\ KOH + 2\ C \rightarrow 2\ K + 3\ H_2 + 2\ K_2CO_3 \quad (1)$$

$$K_2CO_3 + C \rightarrow K_2O + 2\ CO \quad (2)$$

$$K_2O + C \rightarrow CO + 2\ K \quad (3)$$

During a low-temperature heat treatment, KOH permeates into the inner carbon layers to form K_2O, which is reduced back to K at a high temperature by the dehydration reaction. The reduction of K_2O proportionally reduces the carbon content, which gives rise to pores within the CAs. The reduced K permeates into the carbon and forms compounds between the layers while enlarging the inner space of the CAs, *i.e.*, KOH affects and changes the inner structure of the CAs, which is presumably the reason for the disappearance of the carbon-specific peaks.[28]

The pore structure of the activated CAs was investigated by measuring the isothermal adsorption-desorption curves of nitrogen gas, as shown in Figure 3. The untreated and KOH-treated CAs showed Type I and Type IV Langmuir N_2

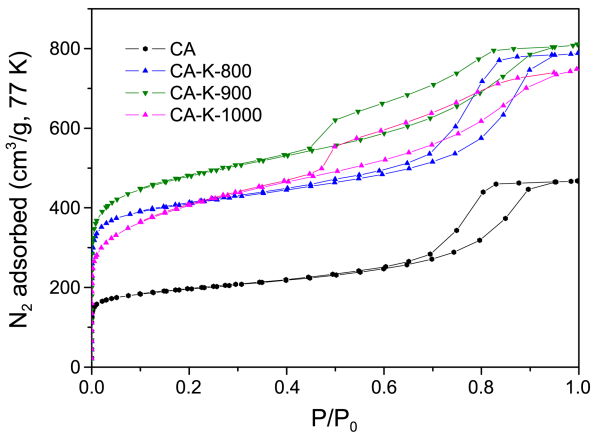

Figure 3. N_2 adsorption/desorption isotherms of the CAs measured at 77 K.

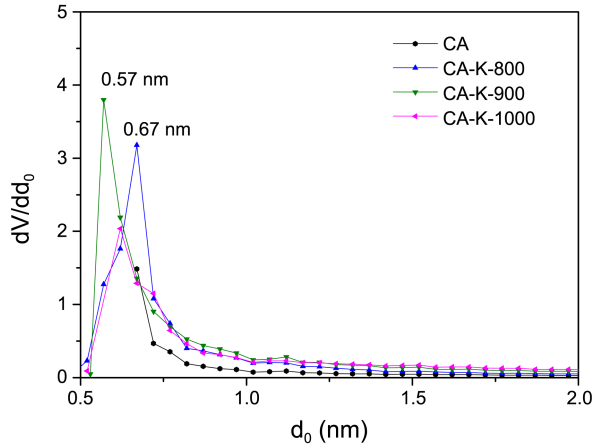

Figure 4. Micropore size distribution of the CAs at activation temperatures of 800-1000 °C.

Table 2. N_2/77 K textural properties of the samples studied

Specimens	S_{BET}[a] (m^2/g)	V_{Total}[b] (cm^3/g)	V_{Micro}[c] (cm^3/g)	V_{Meso}[d] (cm^3/g)	D_P[e] (nm)
CA	623	0.7219	0.1985	0.5234	4.633
CA-K-800	1281	1.2165	0.4769	0.7396	3.7969
CA-K-900	1526	1.2500	0.5105	0.7395	3.2749
CA-K-1000	1340	1.1527	0.3555	0.7972	3.4408

[a]S_{BET}: Specific surface area calculated using Brunauer-Emmett-Teller equation at a relative pressure range of 0.03-0.22. [b]V_{Total}: Total pore volume estimated at a relative pressure $P/P_0 = 0.990$. [c]V_{Micro}: Micropore volume determined from the subtraction of mesopore volume from total pore volume. [d]V_{Meso}: Mesopore volume determined from the Barrett-Joyner-Halenda (BJH) equation. [e]D_p: Average pore diameter

adsorption isothermal curves, respectively. Micropores with a size less than 2 nm were observed under a relative pressure (P/P_0) of 0.1 in the Type I isotherm. The number of micropores increased with increasing activation temperature. The highest numbers of micropores were observed for CA-K-900. Above relative pressure (P/P_0) of 0.4 in Type IV isotherms, midsize pores were found, and the highest numbers of midsize pores were observed for CA-K-900 in the Type IV isotherm.

The pore size distribution (PSD) of the prepared activated CAs was calculated using the H-K formula. Figure 4 shows the distribution of micropores and the average pore size and other pore characteristics are listed in Table 2. As shown in Figure 4, after the activation, all samples had formed micropores, but CA-K-900 formed the largest number of ultramicropores, in particular in the range of 0.5-0.7 nm.

Figure 5 shows the mesopore size distribution in the range of < 50 nm. The pores of CA-K-800 through CA-K-1000 fall in the range of the mesopores, which is most frequently in the pores range of 3-4 nm with increasing the activation temperatures. There was a slight shift in the peaks towards the left to direction with increasing activation temperature. The specific surface area of the activated CAs increased from 1281 for CA-K-800 to 1526 m^2/g for CA-K-900, and the largest specific surface area were obtained for CA-K-900. Accordingly, the micropore volumes increased from

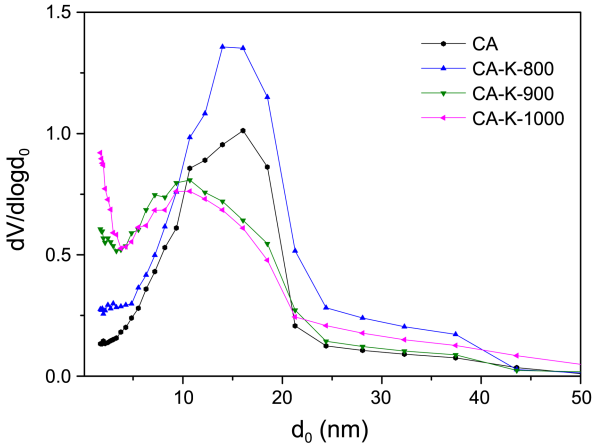

Figure 5. Mesopore size distribution of the CAs at activation temperatures of 800-1000 °C.

0.2696 for CA-K-800 to 0.5105 cm^3/g for CA-K-900 as the temperature increased, thereby increasing the volume of the total pores as well. For CA-K-1000, the gaps within the carbon of the activated CAs became too big to hold the structure because of which the total pore volume, and specific surface area reduced to 1.1527 cm^3/g and 1340 m^2/g, respectively.

Characteristics of CO_2 Adsorption by Activated CAs. The CO_2 adsorption behaviors for the all samples prepared in this study were measured at a stable temperature of 298 K, and the results are shown in Figure 6. The CO_2 adsorption capacities of CA-K-800, CA-K-900, and CA-K-1000 were determined to be 9.3, 10.9, and 7.5 wt %, respectively. The CO_2 adsorption capacity was increased gradually with decreasing pore size to the CA-K-900 sample, whereas the CO_2 adsorption capacity of the CA-K-1000 sample showed no close association. This demonstrates that the CO_2 adsorption capacity of the CA samples depends on the ultramicropore size distribution.

In general, gas adsorption increases when more micropores are generated on an adsorbent. A molecule capable of

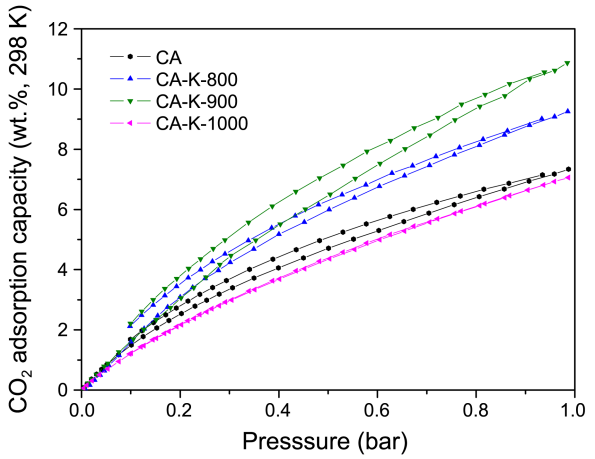

Figure 6. CO_2 adsorption isotherms of CAs measured at 1 bar and 298 K.

a gas-solid interaction works by a strong van der Waals force. Therefore, gas adsorption capacity is improved by a higher adsorption binding energy with increasing number of micropores.[29]

Micropore volumes decreased from 0.5105 cm^3/g for CA-K-900 to 0.3555 cm^3/g for CA-K-1000. The specific surface area decreased from 1526 m^2/g for CA-K-900 to 1340 m^2/g for CA-K-1000. The CO_2 adsorption capacities reduced from 10.9 to 7.5 wt % on going from CA-K-900 to CA-K-1000. The results demonstrate that the CO_2 adsorption volume was the highest for CA-K-900 owing to the increase in the specific surface area with the development of micropores. From the low value of the (002) peak, which represents a carbon-carbon bond, in the XRD pattern of CA-K-1000, it could be confirmed that its carbon layers had collapsed. In addition, the SEM images of CA-K-1000 showed structural changes due to the collapse of carbon layers, this leads to the reduction in the pore volume and, consequently, the CO_2 adsorption capacity.

Conclusions

Carbon aerogels (CAs) were prepared and activated with varying activation temperatures of 800-1000 °C. The effects of different activation temperatures on CO_2 adsorption were studied. The specific surface area of the activated CAs increased from 1281 m^2/g for CA-K-800 to 1526 m^2/g for CA-K-900, which was the largest specific surface area obtained. Moreover, as the activation temperature increased, the total pore volume increased from 0.7219 cm^3/g for the untreated CA to 1.2500 cm^3/g for CA-K-900. The micropore volume increased from 0.1985 cm^3/g for the untreated CA to 0.5105 cm^3/g for CA-K-900. These results indicate that the highest total pore volume and number of micropores were obtained for the CA activated at 900 °C; the values for both these parameters decreased for the CA activated at 1000 °C. Furthermore, the CO_2 adsorption volume increased with temperature till 900 °C; however, the CO_2 adsorption decreased at 1000 °C. The specific surface area of activated CAs increased with temperatures owing to the formation of micropores. The activation temperature affected CO_2 adsorption and the optimum temperature for CA activation was determined to be 900 °C.

Acknowledgments. This work was supported by the Korea CCS R&D Center (KCRC) grant funded by the Korea government (Ministry of Science, ICT and Future Planning) (0031985).

References

1. Li, B.; Duan, Y.; Luebke, D.; Morreale, B. *Appl. Energy* **2013**, *102*, 1439-1447.
2. Dinda, S. *Sep. Purif. Technol.* **2013**, *109*, 64-71.
3. Lu, C.; Bai, H.; Wu, B.; Su, F.; Hwang, J. F. *Energy Fuels* **2008**, *22*, 3050-3056.
4. Jang, D. I.; Park, S. J. *Bull. Korean Chem. Soc.* **2011**, *32*, 3377-3381.

5. Bai, B. C.; Kim, J. G.; Im, J. S.; Jung, S. C.; Lee, Y. S. *Carbon Lett*. **2011**, *12*, 236-242.
6. Meng, L. Y.; Park, S. J. *J. Nanosci. Nanotechnol*. **2013**, *13*, 401-404.
7. Meng, L. Y.; Park, S. J. *J. Colloid Interface Sci.* **2012**, *386*, 285-290.
8. Lee, S. Y.; Park, S. J. *J. Colloid Interface Sci*. **2013**, *389*, 230-235.
9. Li, Y.; Sun, N.; Li, L.; Zhao, N.; Xiao, F.; Wei, W.; Sun, Y.; Huang, W. *Mater*. **2013**, *6*, 981-999.
10. Klinthong, W.; Chao, K. J.; Tan, C. S. *Ind. Eng. Chem. Res.* **2013**, *52*, 9834-9842.
11. Meng, L. Y.; Park, S. J. *J. Colloid Interface Sci*. **2012**, *386*, 125-129.
12. Jang, D. I.; Park, S. J. *Fuel* **2012**, *102*, 439-444.
13. Meng, L. Y.; Park, S. J. *Mater. Chem. Phys.* **2012**, *137*, 91-96.
14. Baltrusaitis, J.; Schuttlefield, J.; Zeitler, E.; Grassian, V. H. *Chem. Eng. J*. **2011**, *170*, 471-481.
15. Marques, L. M.; Carrott, P. J. M.; Ribeiro Carrott, M. M. L. *Adsorpt. Sci. Technol*. **2013**, *31*, 223-232.
16. Castilla, C. M.; Hodar, F. J. M. *Carbon* **2005**, *43*, 455-465.
17. Al-Muhtaseb, S. A.; Ritter, J. A. *Adv. Mater.* **2003**, *15*, 101-114.
18. Pekala, R. W. *J. Mater. Sci.* **1989**, *24*, 3221-3227.
19. Lu, X.; Arduini-Schuster, M. C.; Kuhn, J.; Nilsson, O.; Fricke, J.; Pekala, R. W. *Science* **1992**, *225*, 971-972.
20. Gorka, J.; Fenning, C.; Jaroniec, M. *Coll. Surf. A Physicochem. Eng. Asp*. **2009**, *352*, 113-117.
21. Jin, J.; Mitome, T.; Egashira, Y.; Nishiyama, N. *Coll. Surf. A Physicochem. Eng. Asp*. **2011**, *384*, 58-61.
22. Aida, T.; Murayama, I.; Yamada, K.; Morita, M. *J. Power Sources* **2007**, *166*, 462-470.
23. Yorgun, S.; Vural, N.; Demiral, H. *Micropor. Mesopor. Mater.* **2009**, *122*, 189-194.
24. Lee, Y. J.; Park, H. W.; Park, S.; Song, I. K. *J. Nanosci. Nanotechnol.* **2012**, *12*, 6058-6064.
25. Lin, C.; Ritter J. A. *Carbon*. **1997**, *9*, 1271-1278.
26. Ci, L.; Wei, B.; Xu, C.; Liang, J.; Wu, D.; Xie, S.; Zhou, W.; Li, Y.; Liu, Z.; Tang, D. *J. Cryst. Growth* **2001**, *233*, 823-828.
27. Meng, L. Y.; Park, S. J. *Bull. Korean Chem. Soc*. **2012**, *33*, 3749-3754.
28. Park, S. J.; Jin, S. Y.; Kawasaki, J. *J. Korean Ind. Eng. Chem*. **2003**, *14*, 1111-1115.
29. Romanos, J.; Beckner, M.; Rash, T.; Firlej, L.; Kuchta, B.; Yu, P.; Suppes, G.; Wexler, C.; Pfeifer, P. *Nanotechnology* **2012**, *23*, 015401-015408.